IEEE Photonics Journal
An IEEE Photonics Society Publication

Angular Selective Light Filter Based on Photonic Crystals for Photovoltaic Applications

Volume 2, Number 3, June 2010

James G. Mutitu
Shouyuan Shi
Allen Barnett
Dennis W. Prather

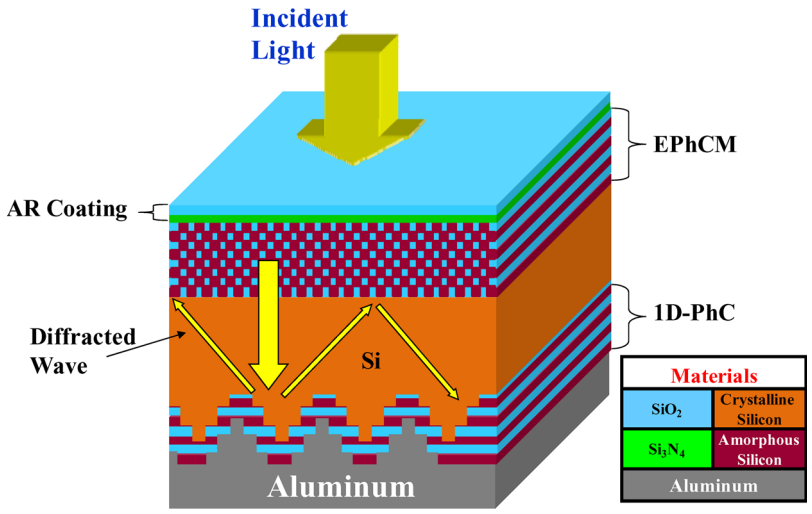

DOI: 10.1109/JPHOT.2010.2050305
1943-0655/$26.00 ©2010 IEEE

IEEE photonics SOCIETY

IEEE

Angular Selective Light Filter Based on Photonic Crystals for Photovoltaic Applications

James G. Mutitu, Shouyuan Shi, Allen Barnett, and Dennis W. Prather

Department of Electrical and Computer Engineering, University of Delaware, Newark, DE 19716 USA

DOI: 10.1109/JPHOT.2010.2050305
1943-0655/$26.00 ©2010 IEEE

Manuscript received March 30, 2010; revised May 4, 2010; accepted May 5, 2010. Date of publication May 12, 2010; date of current version June 11, 2010. Corresponding author: J. G. Mutitu (e-mail: mutitu@mail.eecis.udel.edu).

Abstract: In this paper, we present a new angular selective filter design that is based on photonic bandgap engineering principles. The operation of the filter is based on the occurrence of angular-dependent photonic stopbands and passbands in a photonic crystal structure. Such a filter allows for the propagation of normally incident light while disallowing the propagation of obliquely incident light waves. When the filter is applied to a solar cell structure that consists of a diffraction grating structure on the back surface, a high-efficiency light trap can be formed. Hence, the light-trapping capacity of the new structure is dependent on the photonic band structure of the light filter rather than on refractive optical properties of the active photovoltaic material. This paper presents a model of such a structure and investigates the possibilities afforded by the new structure.

Index Terms: Photonic materials and engineered photonic structures, photovoltaics, diffractive optics, photonic bandgap structures.

1. Introduction

The issue of clean renewable energy sources has, in recent months, expanded from a subject of importance to researchers and environmentalists to one of national interest. It concerns economic progress, the welfare of working families, increasing national security, and saving the environment. To this end, the government proposed its New Energy for America initiative, where "harnessing the power of the sun" was identified as one of the avenues that will champion this endeavor [1], [2]. Hence, it is safe to say that the case for solar electricity has been articulated, at least in part.

The solar electric industry, however, is one that is filled with a myriad of complicated issues that inhibit the industry from reaching its full potential. To make the industry economically viable, there is the need to lower the costs of module production to below $1/watt while at the same time ensuring higher (greater than 15%) module efficiencies [3]. Second, for individual consumers, the ability to incorporate photovoltaic devices for energy production is limited by the amount of space available for installation. This availability of space factor especially affects potential consumers who live in cities, in apartment-style high-rise complexes, where the available real estate for photovoltaic applications is significantly limited. Another application of photovoltaics that has even less real estate available is portable consumer electronics. Portable electronic devices, such as cellular phones and laptop computers, which incorporate rechargeable batteries, are prime markets for photovoltaic devices. Portable solar-powered electronics give consumers the ability to use their gadgets in a larger number of locations, including non-grid-connected remote locations, while also reducing their consumption of grid-connected electrical power.

In the recent past there have emerged a number of new products that incorporate photovoltaic devices, such as the first solar-powered cellular phone made by Samsung, named the "Solar Guru." However, the solar cells used on this and other portable devices are not very efficient; the Solar Guru is reported to need 1 h of solar charging for 5–7 min of talk time [4]. The potential of such applications across a wide range of markets is governed by the energy production capacity and cost of the photovoltaic devices. This means that, in effect, the solar electric market for non-commercial individual consumers is based on available real estate. Hence, the need for very high efficiency solar cells has become even more pronounced. The quest toward achieving very high efficiency solar cells involves the incorporation of multiple technologies into a single structure in order to maximize the device efficiency. The current state-of-the-art cells incorporate multiple-junction, full-solar-spectrum-utilization device technologies [5], [6]. In these types of architecture it is of utmost importance to maximize on the performance of each individual element. Hence, the work in this paper focuses on specifically optimizing the performance of crystalline silicon (c-Si) solar cells for the multiple-stack architecture described in [5], [6]. The c-Si cell in this architecture is placed below a gallium arsenide cell (with a bandgap of 1.43 eV) and would thus operate in the 867–1100 nm wavelength band. Thus, the structures presented in this manuscript are designed and analyzed specifically for this wavelength band. In this wavelength region, c-Si only absorbs 7.8% of the incident irradiance, hence the need for light trapping.

To meet all the aforementioned challenges, various avenues of exploration have come to the fore. One technology that has generated considerable interest is thin-film solar cells (TFSCs). By their very nature, TFSCs reduce the amount of material needed in manufacturing each solar cell and thus ultimately reduce the cost per watt of output power. However, the reduction in active photovoltaic material also compromises the cell efficiency and consequently the need for optimized optical design arises [7], [8]. Light trapping affords the capacity to reduce the thickness of the active solar cell material while still maintaining, in theory, similar absorption characteristics as those of thicker cells. This means that with the addition of an appropriate light-trapping scheme, the efficiencies of standard commercial cells can be achieved with much less material.

In the recent past, there has arisen significant interest in the amalgamation of photovoltaic and photonic engineering concepts to increase the light-trapping performance of TFSCs. This interest has led to, among other concepts, the investigation of photonic crystals (PhCs) as components of the solar cell light-trapping architecture [9], [10]–[16]. Our early work on the subject focused on designs that incorporated antireflective coatings (AR coatings), along with diffractive gratings incorporated into a wavelength-selective light filtering 1-D PhC, at the back surface [12], [13]. Such designs made use of total internal reflection (TIR) conditions within the active solar cell region, which were brought about by the redirection of incoming light due to diffraction from the reflective integrated PhC diffractive gratings. In the new design, we employ an engineered photonic crystal material (EPhCM) which is designed to allow the transmission of normally incident solar light waves but totally reflect the obliquely incident waves from within the solar cell.

2. Design Based on Engineered PhCs

To understand the governing physical phenomena behind the EPhCM, it is necessary to describe PhCs. A PhC is a periodic arrangement of dielectric or metallic materials with a lattice constant comparable to the wavelength of an electromagnetic wave. The interaction of an electromagnetic wave with a periodic dielectric structure results in an interference pattern that allows for some light to propagate or be reflected from the different layers of the structure. This phenomenon is described in a band structure, which maps out the range of frequencies that are permitted to propagate and those that are disallowed. The parameters that determine the band structure are the refractive index contrast and thicknesses of the corresponding layers [12], [13], [17]. A PhC can be designed in such a way that normally incident light falls within the passband of the PhC (range of frequencies allowed to propagate through the structure), and obliquely incident light falls within the stopband (range of frequencies that do not propagate through structure). This specially engineered PhC is what we refer to in this manuscript as the EPhCM, and its function is illustrated in Fig. 1. The EPhCM structure is

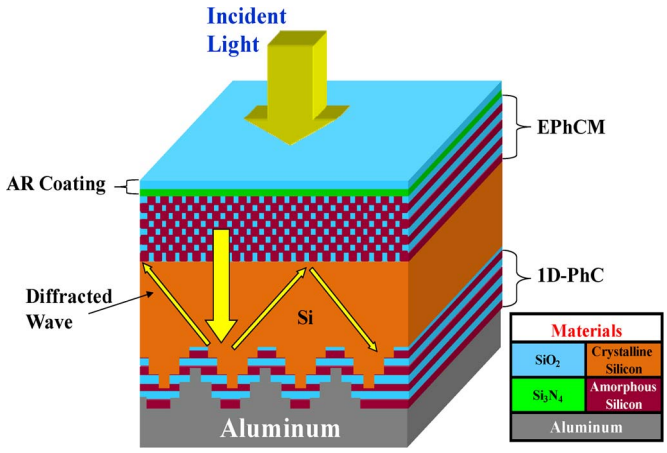

Fig. 1. Design of solar cell structure that incorporates an EPhCM and double diffraction grating. The diffracted waves are trapped within the active silicon region because of the stopbands in the EPhCM structure.

directly applicable to the designs described in our previous work [12], [13], in that it prevents optical losses that occur due to out-coupling of light from the solar cell structures. This comes about because, in solar cell structures with symmetric gratings, such as rectangular binary gratings, diffracted orders propagate to the left and right of the grating with the same angle (for the same positive and negative orders) and same magnitude. With the EPhCM designed for only normally incident light waves, any diffracted waves that are obliquely incident on the EPhCM will be reflected due to the stopband of the structure. Hence, the TIR conditions are a consequence of reflection, or non-admittance, of obliquely incident light waves, rather than primarily of the effects of the refraction of light, as illustrated in Fig. 1. This effect also increases the design tolerance of the diffraction grating, since the critical angle of the active photovoltaic material, c-Si here, is no longer a limiting factor in the grating design process.

In this paper, we focus our attention on c-Si solar cells: all designs presented are based on c-Si as the active photovoltaic material. c-Si is our chosen material because it has high device efficiency potential, is abundant, is stable, and has well-established technology, which is pertinent to the development of nanoscale light-trapping structures. At short wavelengths of light, c-Si is strongly absorbing, as can be affirmed by the high values of its absorption coefficient at shorter (UV–Visible) wavelengths. However, due to its indirect bandgap, c-Si is weakly absorbing in the near infrared regime of the solar spectrum, which can be attested by the increase in absorption length (reciprocal of absorption coefficient) from 11 μm at 800 nm to over 3 mm at 1100 nm [18]. This effect makes it difficult to achieve high-performance thin-film devices with thicknesses in the order of a few micrometers. Consequently, there is a pronounced need for specialized light-trapping architecture that increases the optical path length of light within the solar cell and thereby increases the overall cell efficiency. This specialized need gives rise to our utilization of PhC structures (EPhCM in this case) in the design of high-efficiency light-trapping schemes.

When considering sub-wavelength design geometries, in addition to the inclusion of dispersion based PhC structures, rigorous electromagnetic tools are required to solve for the various fields and effects within the design structure. To this end, we utilize a host of computational electromagnetic tools to model the interaction of electromagnetic waves with these complex design geometries. To understand the interaction of electromagnetic waves with the periodic PhC elements, we employ the plane-wave method and finite-difference time-domain (FDTD) method, which are both explained in great detail in [17]. In addition, we employ the design tools we used in previous endeavors, (i.e., the particle swarm optimization (PSO) method and the scattering matrix (S-Matrix) method) to model and optimize the design performance [12], [13].

The EPhCM structure is a PhC (2-D PhC in this case) in which the dispersion properties are engineered in such a way as to allow the propagation of light incident at certain angles while disallowing the passage of obliquely incident light. In designing the EPhCM, we use a square lattice of

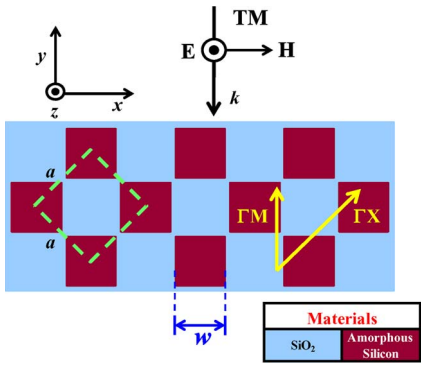

Fig. 2. Showing parameters of the EPhCM; the lattice constant *a* and the width of the a-Si squares *w* are shown. The figure also shows an incident TM polarized wave at the top of the structure.

square shaped dielectric columns made of amorphous silicon (a-Si), with $w/a = 0.45$, where w is the width of the square "rods," and a is the lattice constant of the EPhCM embedded in a slab of SiO_2, as shown in Fig. 2. The lattice constant is equal to the product of the design wavelength and the normalized frequency; thus, for a design wavelength of 867 nm and a normalized frequency of 0.242 c/a, $a = 210$ nm. The width of the square rods w is therefore $0.45a = 94.5$ nm. The period of the EPhCM is 297 nm; this is the diagonal of the green-dashed square in Fig. 2. We choose square shaped columns to enable accurate further analysis using the S-Matrix method, in which square and rectangular geometries are easily described and analyzed. It is worth noting that the S-Matrix method, when used with multiple stacked layers, regardless of the thickness of each layer, is more efficient than volumetric numerical electromagnetic techniques, such as the finite element method or FDTD. The unit cell in this case is a square lattice of square-shaped columns which are rotated by an angle of 45°; thus, the equifrequency contours (EFCs) appearing at the edges, in Fig. 3, correspond to normally incident light. The entire structure is then rotated again by 45° to ensure that the propagating modes occur at normal incidence. The resultant structure assumes a "chess-board" pattern as shown in Fig. 2.

The rationale behind the operation can be understood by considering the EPhCM as consisting of an array of periodic squares of high-index materials (a-Si in this case) embedded in a slab of a lower-index material (SiO_2 in this case). The relationship between the frequency ν and its associated wave vector $\mathbf{k}$ is described in a dispersion diagram. The dispersion diagram is achieved by solving Maxwell's equations, as an eigenvalue problem, through the use of computational electromagnetic simulation methods such as the plane wave method and FDTD [17]. The solutions obtained can be represented as a dispersion surface; this is achieved by computing all the eigenfrequencies for wave vectors at all k points within the irreducible Brillouin zone and then applying the appropriate symmetry operations. The shapes of the dispersion surfaces are dependent on the fill-factor, lattice type, pitch, or index of refraction. By taking cross sections of the dispersion surfaces at constant frequencies, EFCs are obtained; some EFCs for transverse magnetic (TM) polarization of the EPhCM structure are shown in Fig. 3. The shaded region (in Fig. 3) shows the range of angles in which an incident wave will be allowed to propagate through the EPhCM, which is mainly in the Γ-M direction. The direction of energy flowing in a propagating light wave is described by the group velocity which is given in

$$\mathbf{v}_g = \nabla_k \omega(\mathbf{k}). \tag{1}$$

The group velocity $\mathbf{V}_g$ is a vector pointing in the direction of steepest ascent of the dispersion surface and is thus perpendicular to the EFC.

In 2-D PhCs, the fields can by divided into two polarizations by symmetry, namely transverse electric (TE) and TM [19]. In TE mode, the electric field is in the PhC plane (in the $x-y$ plane), and the magnetic field is perpendicular to the plane (z plane). In TM mode, the magnetic field is in the $x-y$ plane of the PhC, while the electric field is perpendicular (in the z plane) to the plane $(x-y)$.

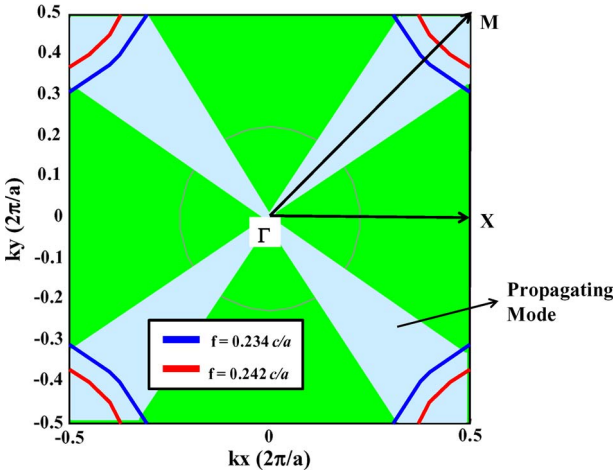

Fig. 3. Equifrequency contours for the EPhCM structure, with the normalized frequencies of the EFCs being 0.234 c/a (blue EFC), and 0.242 c/a (red EFC) The shaded area shows the variation in the admissible angles for the incident wave vector.

The band structures for the two polarizations, TE and TM, can be completely different. In a structure in which high-index "rods" are embedded in a lower-index medium, there needs to exist thin vein lines along which the electric field lines can run (i.e., of the lower index dielectric material). Thus, the EPhCM structure is best suited for TM polarized waves. Since Maxwell's equations are scale invariant, the solution obtained, with the EFC, can be applied to any wavelength by choosing the appropriate value for the lattice constant [19].

We use the FDTD method to simulate the wave propagation through the EPhCM structure, and the results are shown in Fig. 4. Fig. 4(a) depicts a normally incident plane windowed wave that propagates through the EPhCM structure and reaches the detectors labeled DN1, DN2, and DN3. Fig. 4(b) shows the same EPhCM structure, with light incident at 45°, from the solar cell active region; the wave is reflected by the EPhCM structure, and almost nothing propagates to the detectors labeled DO1, DO2, and DO3. Fig. 4(c) shows the amplitude of the wave at the detectors (green crosses) transmitted from the normally incident wave of Fig. 4(a). Fig. 4(d) shows the amplitude of the wave transmitted from obliquely incident wave of Fig. 4(b).

3. Results and Analysis

We quantify the resultant device performance using a number of performance metrics such as the short circuit current (J_{sc}) and band-edge enhancement factor (EF), which are described in [12] and [13]. The J_{sc} is given

$$J_{sc} = \frac{q}{hc} \int_{\lambda} \lambda' A(\lambda') Irrd(\lambda')\, d\lambda' \tag{2}$$

where J_{sc} is the short circuit current density, q is the charge on an electron, h is Planck's constant, c is the speed of light, λ is the wavelength, A is the absorption of the silicon structure, and $Irrd$ is the solar irradiance spectrum [7], [12], [13].

The EF is the ratio of the average absorption of a modified silicon solar cell to the average absorption of a silicon cell with no light-trapping structures as in

$$EF(\lambda) = \frac{\int_{\lambda}^{\lambda=1100} A_E(\lambda') Irrd(\lambda')\, d\lambda'}{\int_{\lambda}^{\lambda=1100} A_s(\lambda') Irrd(\lambda')\, d\lambda'} \tag{3}$$

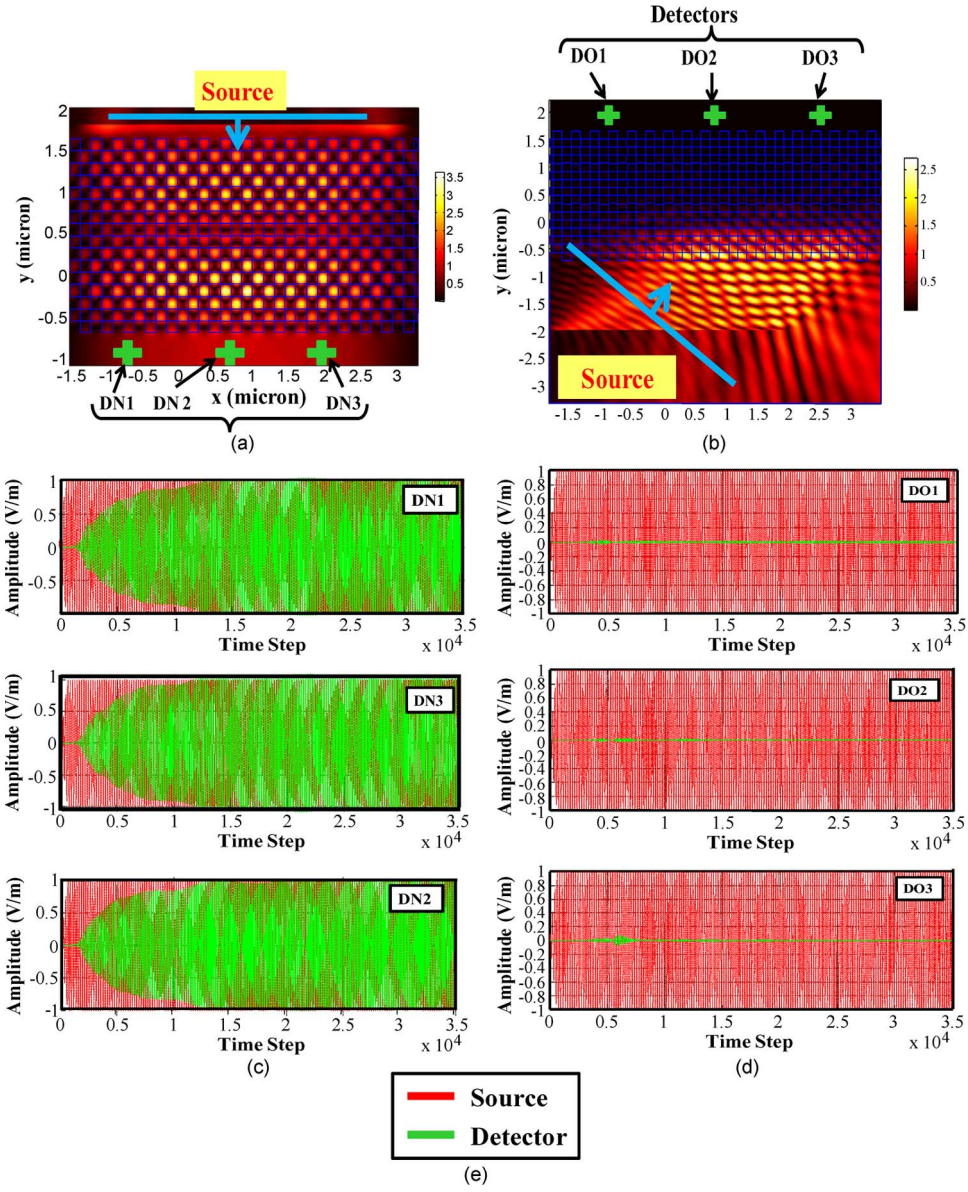

Fig. 4. (a) FDTD simulation results showing the propagation of normally incident light waves through the EPhCM structure; (b) shows the reflection of obliquely (45°) light; (c) shows the amplitude of the incident wave (red plot) that reaches the detectors (green plot) DN1, DN2, and DN3 below the EPhCM structure for normally incident light as shown in (a); (d) shows the plot of the amplitude of the source that reaches the detectors DO1, DO2, and DO3, of (b); (e) is the figure legend for sections (c) and (d).

where the value A_E represents the absorption characteristics of an enhanced structure, i.e., with the light-trapping structures incorporated, A_S represents the absorption of a silicon structure with no light-trapping structures at the top or bottom surfaces.

It is important to note that use of the term band-edge EF is a bit of a misnomer because the term was actually used to show the enhancement in a silicon cell placed in the multiple device stack architecture described in [4] and [5], i.e., below a gallium arsenide cell (with a bandgap of 1.43 eV). We continue with the use of this term for purposes of consistency, continuity and comparison with the designs that we worked on before. We calculate the absorption of an enhanced structure for a

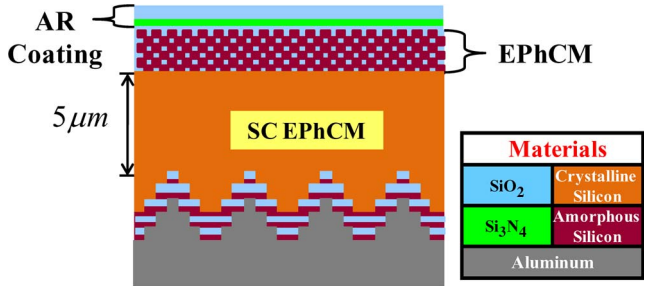

Fig. 5. Design schematic of the new SC EPhCM structure.

wavelength range near the silicon band edge (in this case 867–1100 nm) and normalize it to the absorption characteristics of a cell without any light-trapping structures.

The structure analyzed in this paper is a continuation from a previous effort presented in [13]. This time around, the design process differs in that we utilize spectroscopic ellipsometry to acquire the optical properties of the materials which are then used in the simulation analysis. We use actual samples of materials deposited using an in-house plasma enhanced chemical vapor deposition (PECVD) system and c-Si wafers to acquire the optical data. This process gives us a higher level of accuracy in the results presented than was previously possible; hence, the proximity of these simulation results to real device performance is higher than those from before.

The new structure is similar to HDM 3, with the main difference stemming from the addition of the EPhCM, and hence, we refer to the new structure as SC EPhCM, i.e., short for Solar Cell with EPhCM, as shown in Fig. 5. The structure has a double layer AR coating that consists of a top silicon dioxide (SiO_2) layer and a layer of silicon nitride (Si_3N_4). The thickness of the c-Si in the designs is maintained at 5 μm, mainly for purposes of consistency with the structures presented in [12], [13]. The SC EPhCM also has a 1-D PhC structure that consists of alternating a-Si and SiO_2 layers placed at the back surface. The 1-D PhC layers are cut through to make the triangular gratings. The grating consists of the 1-D PhC structure overlapping an aluminum structure. The 1-D PhC grating consists of four alternating layers above the aluminum grating and four alternating layers interdigitated with the aluminum grating as shown in Fig. 5. The thickness of each period of the metallic triangular grating corresponds to the thicknesses of the a-Si and SiO_2 layers in the 1-D PhC. Hence, with four alternating layers that correspond to the metallic grating, the metal has eight periods [13]. The periods of the four alternating 1-D PhC layers for the top grating are 90 nm, 270 nm, 450 nm, and 630 nm. The eight periods of the aluminum layer grating is calculated by multiplying each factor in the list of 0.1, 0.2, . . ., 0.8 by 900 nm. At the very base of the design, a flat aluminum layer of 1 μm thickness is added. A summary of the optimal design parameters is presented in Table 1.

The dispersion engineering of the PhC (shown in Section 2) was done for a single wavelength. However, when considering a broader wavelength band (867–1100 nm) coupled with other considerations such as impedance matching, dispersion properties over the wavelength range, and the influence of the other features in the SC EPhCM the problem becomes much more complex. Hence, It is worthwhile to perform an optimization of the EPhCM design parameters and, in particular, the square rod size w. The optimal size w of the square rods (as shown in Fig. 2) is found to be 93 nm (EPhCM period is still 297 nm), which is close to the 94.5-nm design size that was obtained in Section 2 of this paper; the difference arose due to all the aforementioned reasons for optimization.

The design tolerance of the rod width w is $93 + 7 / -13$ nm. The J_{sc} performance drops off slightly for wavelengths of up to 13 nm below 93 nm; however, above 100 nm and toward 120 nm, the performance drops off considerably; the J_{sc} drops by 15% at 120 nm, as shown in Fig. 6. As w tends toward 120 nm, the effect of the EPhCM is more localized at the c-Si band edge (closer to 1100 nm), where photons have less energy (and is less so over the rest of the 867–1100 nm region).

We utilize the S-Matrix method to analyze the performance of the SC EPhCM design and compare the results with those of a base case with no light trapping as well as to the maximum J_{sc} available. In this simulation, both TE and TM polarizations are considered; the absorption and

TABLE 1
Optimal Design Parameters for HDM 3 and SC EPhCM

Design Structure	Optimal Design Parameters
AR coating top layer (SiO_2)	99 nm
AR coating second layer (Si_3N_4)	49 nm
Silicon active layer	5 μm
Triangular grating period (both 1D-PhC and Aluminum)	900 nm
1D-PhC SiO_2 layer thickness	170 nm
1D-PhC a-Si layer thickness	79 nm
Triangular grating thickness (both 1D-PhC and Aluminum)	996 nm
Aluminum back reflector thickness	1 μm

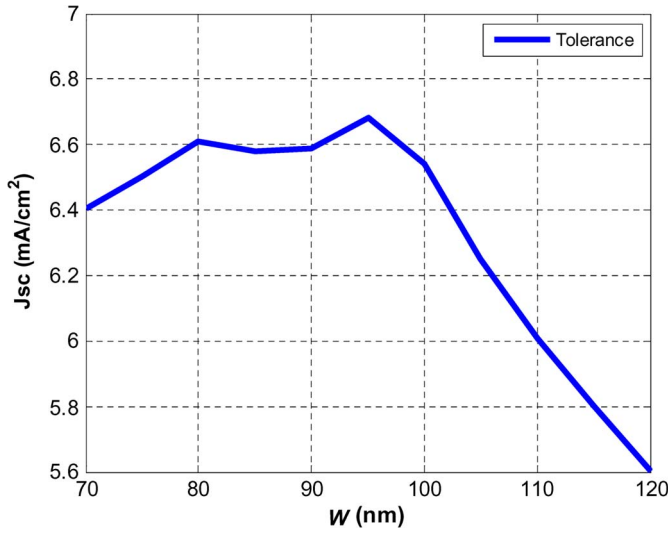

Fig. 6. Tolerance analysis of the squared rod width w of the EPhCM structure in terms of the J_{sc} characteristics at the silicon band edge (867–1100 nm).

subsequent J_{sc} and EF characteristics are achieved by taking the mean of the characteristics obtained from the two polarizations. The band edge J_{sc} (867–1100 nm) of the EPhCM structure is 6.7 mA/cm^2, which is an increase of more than 6 mA/cm^2 over a structure with no light trapping, as shown in Fig. 7. It is worthy to note that at about 1100 nm, the base case exhibits close to zero absorption, and hence, the enhancement in J_{sc} characteristics is very significant.

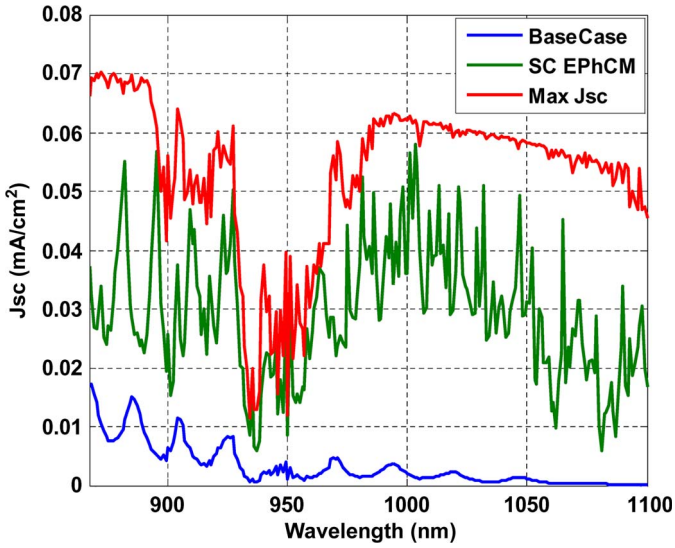

Fig. 7. Simulated short circuit current characteristics of the new SC EPhCM structure (green plot) as compared with a bare silicon solar cell with no light trapping (blue plot) and maximum available J_{sc} (red plot).

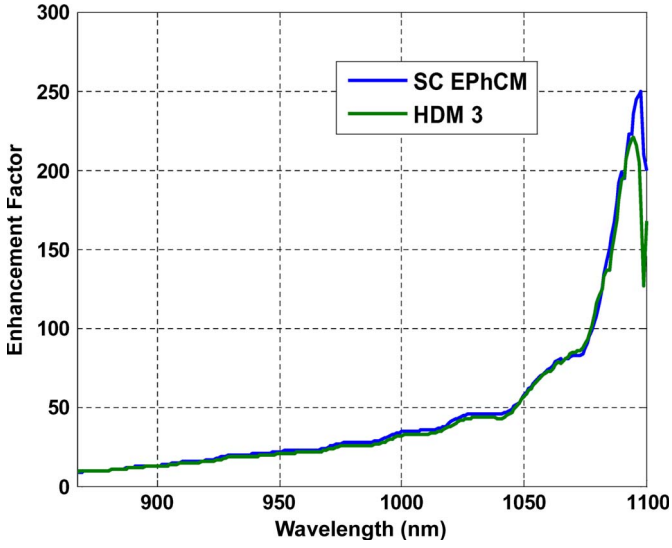

Fig. 8. Enhancement factor comparison of the SC EPhCM structure (blue plot) and the HDM 3 structure which does not include the EPhCM (green plot). The SC EPhCM structure enhances the absorption of light by a factor of almost 250 at the silicon band edge.

To investigate the angular dependence of the incident wave, the Jsc performance is evaluated by varying the incident angle from the normal to 45°. The J_{sc} performance of the solar cell is consistent for incident light that varies by up to 7° from the normal to the solar cell surface; beyond this point, the performance begins to drop. At 15° from the normal, the J_{sc} is 10% less than in the case of normally incident light. This 10% drop occurs because a larger stopband opens at 15°. However, the effect of the stopband is small, i.e., 10%, due to the small number of wavelengths near the silicon band edge, i.e., the wavelength range considered in this analysis (867–1100 nm).

To characterize the absorption properties of the EPhCM in the simulation, the a-Si used in the simulations is assumed to be lossless; hence, the absorption contributions are only from the c-Si active layer. In the case of a real device structure, the absorption from a-Si would still be low

because the fill factor of a-Si in the EPhCM is less than 33%. Furthermore, a-Si is not a very strong absorber of wavelengths near the c-Si band edge (around 1100 nm), i.e., when compared with c-Si.

We finally compute the EF of the structure, i.e., comparing the absorption characteristics of the light-trapping enhanced structure, with those of the base-case structure, and in addition, we compare the enhancement with that of the HDM3 structure. We see that the SC EPhCM structure increases the absorption characteristics by a factor of 250 above that of a structure with no light trapping close to 1100 nm, as shown in Fig. 8. The HDM3 structure increases the characteristics by a factor of 220 at the same wavelength. The high EF of the EPhCM fitted solar cell is a clear indicator of the benefits obtained by using the EPhCM structure in a TFSC.

4. Conclusion

The SC EPhCM structure solves the fundamental problem of the out coupling of light that is obliquely incident on the front surface, of the solar cell, from within the active region. This out coupling of light is limited by the angular selectivity of the EPhCM structure, and hence, the absorption characteristics are greatly increased by up to a factor of 250 close to 1100 nm. The J_{sc} characteristics of this structure are 6.7 mA/cm^2 compared with about 0.8 mA/cm^2 for a structure with no light trapping, i.e., in the 867–1100-nm range. Hence, the new design structure presented in this paper is well suited for high efficiency multistack solar cell design architecture.

References

[1] B. Obama, *Transcript: Obama's Inaugural Address*, 2009.
[2] B. Obama and J. Biden, *New Energy for America*, 2009.
[3] K. R. Catchpole, M. J. McCann, K. J. Weber, and A. W. Blakers, "A review of thin-film crystalline silicon for solar cell applications. Part 2: Foreign substrates," *Sol. Energy Mater. Sol. Cells*, vol. 68, no. 2, pp. 173–215, May 2001.
[4] *Samsung Introduces the World's First Solar Powered Mobile Phone*, Samsung, 2009, p. 1. [Online]. Available: http://www.samsung.com/in/news/newsRead.do?news_seq=13759&gltype=localnews
[5] A. Barnett, C. Honsberg, D. Kirkpatrick, S. Kurtz, D. Moore, D. Salzman, R. Schwartz, J. Gray, S. Bowden, K. Goossen, M. Haney, D. Aiken, M. Wanlass, and K. Emery, "50% efficient solar cell architectures and designs," in *Proc. IEEE 4th WCPEC*, 2006, pp. 2560–2564.
[6] A. Barnett, D. Kirkpatrick, C. Honsberg, D. Moore, M. Wanlass, K. Emery, R. Schwartz, D. Carlson, S. Bowden, D. Aiken, A. Gray, S. Kurtz, L. Kazmerski, M. Steiner, J. Gray, T. Davenport, R. Buelow, L. Takacs, N. Shatz, J. Bortz, O. Jani, K. Goossen, F. Kiamilev, A. Doolittle, I. Ferguson, B. Unger, G. Schmidt, E. Christensen, and D. Salzman, "Very high efficiency solar cell modules," in *Prog. Photovoltaics Res. Appl.*, vol. 17, pp. 75–83, 2009.
[7] R. Brendel and A. Goetzberger, *Thin-Film Crystalline Silicon Solar Cells: Physics and Technology*. Weinheim, Germany: Wiley-VCH, 2003, p. 287.
[8] B. Sopori, "Thin-film silicon solar cells," in *Handbook of Photovoltaic Science and Engineering*, A. Luque and S. Hegedus, Eds. Chichester, U.K.: Wiley, 2003.
[9] D. Zhou and R. Biswas, "Photonic crystal enhanced light-trapping in thin film solar cells," *J. Appl. Phys.*, vol. 103, no. 9, p. 093102, May 2008.
[10] L. Zeng, Y. Yi, C. Hong, B. A. Alamariu, J. Liu, X. Duan, and L. C. Kimerling, "New solar cells with novel light trapping via textured photonic crystal back reflector," in *Proc. MRS Fall Meeting*, Nov. 28, 2005–Dec. 1, 2006, pp. 251–256.
[11] L. Zeng, Y. Yi, C. Hong, J. Liu, N. Feng, X. Duan, L. C. Kimerling, and B. A. Alamariu, "Efficiency enhancement in Si solar cells by textured photonic crystal back reflector," *Appl. Phys. Lett.*, vol. 89, no. 11, p. 111111, Sep. 2006.
[12] J. G. Mutitu, S. Shi, C. Chen, T. Creazzo, A. Barnett, C. Honsberg, and D. W. Prather, "Thin film silicon solar cell design based on photonic crystal and diffractive grating structures," *Opt. Express*, vol. 16, no. 19, pp. 150 238–15 248, Sep. 2008.
[13] J. G. Mutitu, S. Shi, C. Chen, A. Barnett, C. Honsberg, and D. W. Prather, "Light trapping designs for thin silicon solar cells based on photonic crystal and metallic diffractive grating structures," in *Proc. 34th IEEE Photovoltaic Spec. Conf.*, 2009, pp. 000579–000583.
[14] J. M. Gee, "Optically enhanced absorption in thin silicon layers using photonic crystals," in *Proc. 29th IEEE Photovoltaic Spec. Conf.*, May 19–24, 2002, pp. 150–153.
[15] J. M. Gee, J. B. Moreno, S.-Y. Lin, and J. G. Fleming, "Selective emitters using photonic crystals for thermophotovoltaic energy conversion," in *Conf. Rec. 29th IEEE Photovoltaic Spec. Conf.*, 2002, pp. 896–899.
[16] R. Biswas and Z. Dayu, "Enhancing light-trapping and efficiency of solar cells with photonic crystals," in *Proc. MRS Spring Meeting*, Apr. 9–13, 2007, pp. 35–40.
[17] D. W. Prather, S. Shi, A. Sharkawy, J. Murakowski, and G. Schneider, *Photonic Crystals: Theory Applications and Fabrication*. Hoboken, NJ: Wiley, 2009.
[18] M. A. Green, *Silicon Solar Cells, Advanced Principles and Practice*. Sydney, Australia: NSW: Centre for Photovoltaic Devices Syst., Univ. New South Wales, 1995.
[19] J. D. Joannopoulos, S. G. Johnson, J. N. Winn, and R. D. Meade, *Photonic Crystals: Molding the Flow of Light,* 2nd ed. Princeton, NJ: Princeton Univ. Press, 2008.